



# CHORUS

This is the accepted manuscript made available via CHORUS. The article has been published as:

## Lock-and-key dimerization in dense Brownian systems of hard annular sector particles

Wade D. Hodson and Thomas G. Mason

Phys. Rev. E **94**, 022124 — Published 18 August 2016

DOI: [10.1103/PhysRevE.94.022124](https://doi.org/10.1103/PhysRevE.94.022124)

# Lock-and-Key Dimerization in Dense Brownian Systems of Hard Annular Sector Particles

Wade D. Hodson<sup>1</sup> and Thomas G. Mason<sup>1,2,\*</sup>

<sup>1</sup>*Department of Physics and Astronomy, University of California at Los Angeles, Los Angeles, California 90095 USA*

<sup>2</sup>*Department of Chemistry and Biochemistry, University of California at Los Angeles, Los Angeles, California 90095 USA*

(Dated: July 24, 2016)

We develop a translational-rotational cage model that describes the behavior of dense two dimensional (2D) Brownian systems of hard annular sector particles (ASPs), resembling “C”-shapes. At high particle densities, pairs of ASPs can form mutually interdigitating lock-and-key dimers. This cage model considers either one or two mobile central ASPs which can translate and rotate within a static cage of surrounding ASPs that mimics the system’s average local structure and density. By comparing with recent measurements made on dispersions of microscale lithographic ASPs (P.-Y. Wang and T.G. Mason, *J. Am. Chem. Soc.* 137 15308 (2015)), we show that mobile two-particle predictions of the probability of dimerization  $P_{\text{dimer}}$ , equilibrium constant  $K$ , and 2D osmotic pressure  $\Pi_{2D}$ , as a function of the particle area fraction  $\phi_A$ , correspond closely to these experiments. By contrast, predictions based on only a single mobile particle do not agree well with either the two-particle predictions or the experimental data. Thus, we show that collective entropy can play an essential role in the behavior of dense Brownian systems composed of non-trivial hard shapes, such as ASPs.

PACS numbers: 02.50.-4, 02.70.Rr, 03.65.Vf, 05.10.-a, 05.40.Jc, 05.70.Ln

## I. INTRODUCTION

Homodimer formation has been observed for many different types of molecules, ranging from simple acetic acid [1] to highly complex proteins [2]. In particular, many kinds of proteins, such as the structural coat proteins of viruses [3, 4], and functional enzymes, such as organophosphorous hydrolase [5], form homodimers. In such complex molecular systems, site-specific interactions between monomers, by mechanisms such as hydrogen bonding, can play important roles in dimer formation and stability. By contrast, in Brownian systems of hard colloidal particles, the core shapes of constituent particles and entropy maximization essentially determine the system’s structure and its phase behavior at a certain particle density [6, 7]. For instance, certain particle shapes, which have shape-complementary convex and concave regions, can form composite lock-and-key dimer structures [8]. For hard particles, the simplest type of dimer is the lock-and-key homodimer composed of two identical monomers that mutually interpenetrate, such that the convex portion of one particle enters the concave portion of the other, and vice-versa. Because attractions are absent in hard particle systems, emergent dimer structures can only be maintained over long times in highly crowded environments. In such crowded environments, the osmotic pressure exerted by neighboring particles inhibits the separation of two monomers that have interpenetrated to form a dimer.

Recently, lithographic fabrication of monodisperse dispersions of microscale annular sector particles (ASPs) [8–12] and formation of 2D Brownian systems of particles at high densities that have effectively hard interactions [13, 14] using roughness-controlled depletion attractions [15–18] have enabled direct visualization of dimer-

ization in two dimensions (2D) [9]. Here, we investigate the degree of dimerization of colloidal ASPs in dense 2D Brownian systems using a translational-rotational cage model simulation that is similar to prior cage model simulations of dense Brownian systems of hard rhombs [19, 20] and hard tri-stars [21]. Using a collision detection routine that detects when two ASPs overlap, this simulation enumerates accessible translational and rotational microstates associated with either one or two mobile ASPs surrounded by a static cage of ASPs. This cage structure approximates the average local structure around the central mobile ASP(s) and sets the system’s overall density, similar to cage models of hard spheres [22, 23]. Once these accessible microstates have been determined, key thermodynamic properties of the system can be calculated using basic principles of statistical mechanics [24, 25]. This direct cage modeling approach provides insight into how many local degrees of freedom must be included in order to obtain reasonably accurate predictions for the collective behavior of the dense hard particle system; such insight is not typically provided by many-particle simulations based on Brownian or molecular dynamics [26].

ASPs represent an interesting class of shapes that can range from slender partial rings to pie wedges [27]. Here, we consider a monodisperse dispersion of uniform ASPs that resemble partial rings or “C”-shapes. The shape and size of an ASP can be characterized by the following three parameters: an inner radius  $R_i$ , an outer radius  $R_o$ , and an opening angle  $\psi$ , as defined in Fig. 1(a). Thus, the perimeter of an ASP is set by two aligned concentric circular arcs, each having angular range  $2\pi - \psi$ , and two radial line segments, each having length  $R_o - R_i$ , which connect the ends of the arcs. If  $R_o$  is chosen to set a characteristic particle length scale, then only two dimen-

sionless parameters completely define this class of ASP shapes:  $R_i/R_o$  and  $\psi$ . For certain ranges of these parameters, two monomer ASPs have the capacity to dimerize in mutual lock-and-key configurations. We define mutual lock-and-key dimerization to occur when a portion of one ASP makes contact with an imaginary dashed line extending between the ends of the inner circular arc of the other ASP and vice-versa. Examples of configurations of two proximate ASPs that are not dimerized are shown in Figs. 1(b) and 1(c). However, in the example configuration shown in Fig. 1(d), a portion of one ASP penetrates into the interior cavity of the other ASP and vice-versa, so this is a mutual lock-and-key dimer.

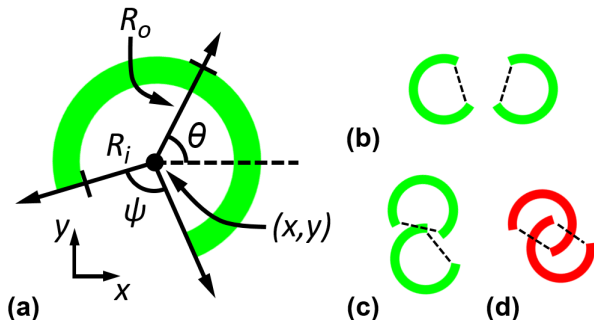


FIG. 1. Schematics of an annular sector particle (ASP) and geometrical condition for mutual lock-and-key dimerization of two ASPs. (a) Shape and size parameters characterizing an ASP:  $R_i$  and  $R_o$  are the inner and outer radii, respectively;  $\psi$  is the opening angle. Coordinates  $x$  and  $y$  define the center of the ASP with respect to the origin of a fixed reference frame.  $\theta$  is its orientation angle, with respect to the  $x$ -axis, based on a ray from the center of the circular arcs to a point that is midway between the ends of the ASP's two arms. (b) Two separate monomer ASPs: no portion of a first ASP intersects with the imaginary dashed line defining the opening boundary of the concave interior of a second ASP, and vice-versa. (c) Two proximate ASPs: a first ASP does intersect with the imaginary dashed line of a second ASP, but the second ASP does not contact the imaginary dashed line of the first ASP. (d) Two proximate ASPs in a mutually interpenetrating lock-and-key dimer configuration. Mutually interpenetrating lock-and-key dimerization occurs when a portion of the perimeter of one ASP intersects with the imaginary dashed line spanning the inner opening of the other ASP, and vice-versa. This geometric definition for dimerization of non-overlapping ASPs can be readily determined using a collision detection routine. This collision detection routine is based on a combination of routines which detect the intersection of two circular arcs, a line segment with a circular arc, and two line segments.

In order to understand how the process of dimerization is influenced by factors such as particle shape and particle density, we implement a model of either one mobile ASP or two mobile ASPs within a fixed cage of neighboring ASPs. In this simulation, the space of accessible positions and angular orientations (*i.e.* accessible microstates) of up to two mobile ASPs is discretized and systematically explored using a collision detection routine, written in Mathematica (Wolfram Research). This

routine also determines which accessible microstates of mobile ASP(s) correspond to mutual lock-and-key dimer configurations of the two central sectors, using a geometric test criterion (see Fig. 1(b)-1(d)). These simulations are executed over a range of particle area fractions,  $\phi_A$ , a quantity related to the average density of the cage, and over a range of values of the particle shape parameters  $R_i/R_o$  and  $\psi$ . This range of shape parameters includes values which match the parameters of ASPs that have been studied experimentally. Although dimers of ASPs are known to have positive and negative chiral senses, here, we model dimerization having only a single chiral sense, since the results for the mirror image of the dimer cage structure are the same. Because the model only relies on an average local short-range structure around a given pair of mobile ASPs, we show that this model for the cage reasonably describes the main thermodynamic features of dense systems of ASPs that form in racemic proportions and are therefore disordered at medium and long range. Although the ASPs are strictly hard particles, dimers can be compressed over a fairly wide range of  $\phi_A$  above the dilute limit, and this leads to an interesting dependence of the equilibrium constant  $K$  of the dimerization reaction as a function of applied 2D osmotic pressure  $\Pi_{2D}$ .

The results of these cage model simulations are given in terms of the total number of accessible microstates  $\Omega$ , and the number of dimer microstates  $\Omega_D$ , for the mobile ASP(s). These values can be used to compute a variety of physical quantities of interest, including the probability of dimerization  $P_{\text{dimer}}$ , the free energy  $F$ , the equilibrium constant  $K$  of the monomer-dimer reaction, and the two-dimensional osmotic pressure  $\Pi_{2D}$  of the thermalized system. Predictions of these quantities are found to match closely with experimental measurements of ASPs, without introducing adjustable parameters. Given this success, we extend results of these cage model simulations to ranges of shape parameters that have not been explored yet experimentally. Moreover, these simulation results demonstrate the importance of accounting for the collective microstates of pairs of mobile ASPs, not just a single ASP, in order to accurately reproduce certain key features of the hard ASP system.

## II. METHODS

In order to study dimerization in systems of ASPs, a translational-rotational cage model is implemented in Mathematica, similar to previous simulations used to study colloidal dispersions of particle shapes such as rhombs [20] and tri-stars [21]. This cage model has been developed to treat either a single central mobile ASP or alternatively a pair of central mobile ASPs. While the two-ASP calculation requires significantly more computational time, it also provides more realistic predictions because it includes the most basic contribution to the collective entropy of the system.

At each different value of  $\phi_A$ , we build a static cage of ASPs that describes the average local structure around a central pair of ASPs, whether dimerized or not. To do this, we define and solve a set of equations that maximizes and equalizes all spacings between densely configured pairs of ASPs that are uniformly positioned, oriented, and dilated, as shown in Fig. 2. Such maximized and equalized spacings between ASPs create a cage configurations that approximately maximize the accessible microstates for cage ASPs if they were allowed to explore different configurations. At higher  $\phi_A$ , the cage ASPs are all dimerized; whereas at lower  $\phi_A$ , the cage ASPs are separated monomers. The cage effectively defines a non-circular central cavity in which the two central mobile ASPs are located, and the accessible microstates of these mobile ASPs are constrained by non-overlap with regard to each other and also the cage ASPs. This approach for defining the cage is taken for computational convenience, since such idealized cage structures, while providing a reasonable approximation of an average cage structure at a certain density, do not incorporate the randomness in chirality and orientation of dimerized ASPs that have been observed in experiments. To reduce computational time, collision detection between central mobile ASPs and certain outer cage ASPs (e.g. uppermost two ASPs and lowermost two ASPs shown in Fig. 2) can be eliminated, except at lower  $\phi_A$  towards the dilute limit, in which case potential collisions with additional outer cage ASPs are also checked. For most values of  $\phi_A$  that we consider, collisions of central mobile ASPs with only eight cage ASPs closest to them need to be checked. Two central mobile ASPs can either have a configuration corresponding to non-interpenetrating monomers [e.g. Fig. 2(a)] or mutually interpenetrating lock-and-key dimers [e.g. Fig. 2(b)]. Examples of cages, showing the central cavity, at several different  $\phi_A$  values are shown in Figs. 2(c)-2(e).

Given two fixed shape parameters  $R_i/R_o$  and  $\psi$ , as well as  $\phi_A$ , the cage model simulation for two mobile ASPs is implemented as follows. First, a spatial configuration of the cage is defined to match the given  $\phi_A$ . We then discretize the six-dimensional space of all possible positions and orientations of the two central ASPs, which yields a set of all possible microstates, some of which might be accessible to the central ASPs without any overlap. For each microstate in this set, a collision detection algorithm determines whether this microstate corresponds to a physically accessible state of the two central ASPs. Here, an accessible state is one for which the central ASPs do not overlap with each other and also do not overlap with any cage ASPs. In addition, if a state is found to be accessible, then it is also tested to determine if the configuration corresponds to a lock-and-key dimer, as defined in Fig. 1(d). The typical output of the cage model simulation, for particular values of  $R_i/R_o$ ,  $\psi$ , and  $\phi_A$ , consists of the total number of accessible microstates  $\Omega$ , and the number of dimer microstates  $\Omega_D$ . The number of monomer (*i.e.* non-dimer)

microstates is simply:  $\Omega_M = \Omega - \Omega_D$ . If desired, the entire list of accessible states in the six-dimensional phase space can also be generated. To preserve accuracy of the results while reducing computational time, we use a finer discretization of the phase space at larger  $\phi_A$ , and a coarser discretization at lower  $\phi_A$ . The resulting numbers of microstates are appropriately rescaled with respect to a fixed six-dimensional volume representing the entire phase space of microstates, so that the results of simulations executed at different discretizations can be meaningfully combined.

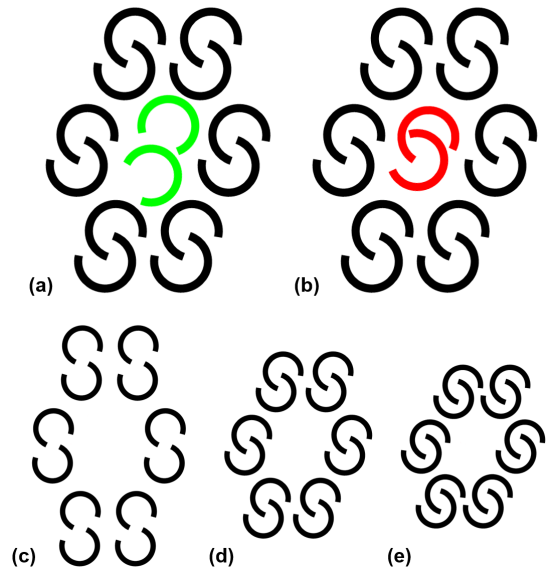


FIG. 2. Cage configurations limiting motion of the central ASPs over a range of values of particle area fractions  $\phi_A$ :  $R_i/R_o = 0.75$  and  $\psi = 95^\circ$ . Static cage ASPs are shown in black. Examples of two central mobile ASPs at  $\phi_A = 0.263$  in: (a) a monomer configuration (green or light gray); (b) a dimer configuration (red or gray). Example cages generated at  $\phi_A$ : (c) 0.180; (d) 0.263; and (e) 0.340.

The cage model simulation is executed over a range of shape parameter values, for  $R_i/R_o$  from 0.65 to 0.8 and for  $\psi$  from  $70^\circ$  to  $120^\circ$ . For each pair of parameters in this range,  $\Omega$  and  $\Omega_D$  are computed for values of  $\phi_A$  between 0.08 and 0.48. Specifically, the simulation is run for  $R_i/R_o = 0.75$  and  $\psi = 95^\circ$ , in order to compare the simulation results with experimental data [9] which has been gathered for ASPs having these shape parameter values. The lower limit of this range of  $\phi_A$  values is set by the escape of central ASPs from the cage, and the upper limit is set by the highest packing density above which overlap of ASPs would always occur.

In addition, for  $R_i/R_o = 0.75$  and  $\psi = 95^\circ$ , a modified version of the cage model that has only a single central mobile ASP is also executed, in order to compare with measurements and results of the two-particle simulations. In this single-particle version, one central ASP is held at a fixed position and orientation corresponding to the cage configuration, while the other cen-

tral ASP is moved and tested for non-overlap. Collision detection is used to determine the numbers of accessible and dimer microstates based only on the motion of a single central ASP. This single-particle simulation has a reduced three-dimensional phase space and runs very rapidly (time  $\sim N^3$ , where  $N$  represents a number of microstates checked along a given dimension of the phase space). However, as a consequence of its basic assumptions, the single-particle simulation does not include collective entropic effects. By contrast, the two-particle simulation, which has a six-dimensional phase space, runs more slowly (time  $\sim N^6$ ), but it does include collective entropic effects at a basic level. For  $R_i/R_o = 0.75$  and  $\psi = 95^\circ$  using the two-particle simulation, the average run time to calculate accessible microstates over the entire cage and classify configurations as monomer or dimer is about five hours on a ThinkServer (Lenovo TS140, Xeon E31225v3 quad-core 3.2 GHz, 4 GB RAM) for fifteen different values of  $\phi_A$ .

### III. RESULTS AND DISCUSSION

As an example to illustrate accessible microstates of central ASPs in a cage of immobile ASPs, we show transparency overlay plots of the accessible monomer and dimer microstates for a single-particle simulation in Figs. 3(a) and 3(b), respectively. Only a fraction of the allowed microstates correspond to mutually interpenetrating lock-and-key configurations. The requirement of *mutual* interpenetration is our strict geometrical definition for dimerization; *both* particles must have portions that cross the dashed lines of the other shown in Fig. 1(d). For two-particle simulations, both central ASPs can move within the static cage. This is difficult to depict clearly, since the transparency overlay plots become smeared over the entire cage.

Over a range of different shape parameters  $R_i/R_o$  and  $\psi$ , we have calculated  $\Omega$  and  $\Omega_D$ , respectively, as a function of  $\phi_A$ . Having determined  $\Omega$  and  $\Omega_D$  through collision detection, equilibrium physical properties of dense 2D Brownian system of ASPs can be computed for different  $R_i/R_o$  and  $\psi$  as a function of  $\phi_A$ . The probability of dimerization is simply  $P_{\text{dimer}} = \Omega_D/\Omega$ , given the assumption of equal *a priori* probabilities for each accessible microstate. Experimentally, this probability can be identified as the fraction of particle pairs which are dimerized. The equilibrium constant  $K$  is defined assuming that separated particle pairs are reactants and dimerized pairs are products. The Gibbs free energy associated with the dimerization reaction of a pair of ASPs is  $\Delta G = -k_B T \ln K$ , where  $k_B$  is Boltzmann's constant and  $T$  is the temperature. For hard-particle systems, this free energy is entirely entropic:  $\Delta G = -T\Delta S$ , where  $\Delta S$  is the entropy change of this reaction. Applying Boltzmann's definition of entropy between monomer and dimer states of the pair yields  $\Delta S = k_B \ln(\Omega_D/\Omega_M)$ . After equating these two expressions for  $\Delta G$  of the reac-

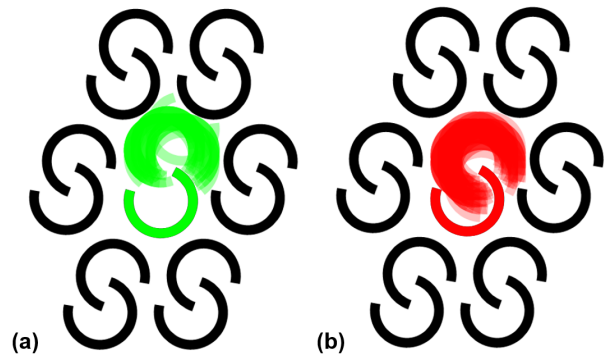


FIG. 3. Accessible microstates of a first central mobile ASP (upper) from the single-particle simulation, for a fixed position and orientation of a second central ASP (lower). Here,  $R_i/R_o = 0.75$ ,  $\psi = 95^\circ$ , and  $\phi_A = 0.263$ . The location and orientation of the fixed ASP, with respect to a coordinate system located at the geometric center of the cage, is given by  $x = -0.05$ ,  $y = -0.5$ , and  $\theta = 300^\circ$ , in units where  $R_o = 1$ . Transparency overlay plots of accessible microstates corresponding to: (a) monomer configurations (green or light gray); (b) dimer configurations (red or dark gray).

tion,  $K$  can be simply deduced as  $K = \Omega_D/\Omega_M$ . Because the phase space is six-dimensional, corresponding to microstates of two particles regardless of whether or not they have dimerized, this form for  $K$ , which can be determined from the simulation results, is equivalent to the experimental  $K$  determined by the law of mass action,  $K = \phi_{A,D}/\phi_{A,M}^2$  using measured area fractions of dimers  $\phi_{A,D}$  and monomers  $\phi_{A,M}$ , respectively, at the same depth in an equilibrated 2D gravitational column. Moreover, the 2D osmotic pressure  $\Pi_{2D}$  as a function of  $\phi_A$  is given by:

$$\Pi_{2D}(\phi_A) = -\frac{k_B T}{2A_p} \phi_A^2 \frac{\partial(\ln \Omega)}{\partial \phi_A}. \quad (1)$$

Here,  $A_p$  is the area of a single ASP, and  $\Omega$  is a function that depends on  $\phi_A$ . Thus, the osmotic equation of state,  $\Pi_{2D}(\phi_A)$ , can be determined by calculating the microstate volumes  $\Omega(\phi_A)$  from the simulation and then differentiating with respect to  $\phi_A$ .

In prior experiments [9, 21], if a system of Brownian hard particles in a 2D column is subject to a uniform gravitational field, then the two-dimensional osmotic pressure can also be expressed in terms of an integral that yields the total effective particle mass above a given height  $z$  in the column:

$$\Pi_{2D}(z) = \frac{k_B T}{A_p} \int_z^\infty \phi_A(z') (dz'/h_g). \quad (2)$$

This integral depends on a particular thermal-gravitational height,  $h_g$ , associated with the initial exponential increase in particle density as a function of depth

within the equilibrated column in the dilute gas-like region. In the prior experiments [9],  $\Pi_{2D}$  has been obtained by extracting  $h_g$  from a curve fit of  $\phi_{A,M}(z)$ , and then integrating using Eq. (2). However, some minor inaccuracy in the experimental  $h_g$  could have resulted from the curve fitting method that was employed, since this value depends on the functional form and the range of  $z$  used in the fit. Here, we re-fit the experimental data for  $\phi_{A,M}(z)$  using a simple exponential form, including only the most dilute gas-like region, and carefully check the correlation coefficient to see how it changes for different ranges of  $z$  used in the fit. From this, we determine a more accurate value of  $h_g = 4.35 \mu\text{m}$ , which is lower than the prior reported value of  $h_g = 5.6 \mu\text{m}$  [9], which included an additional point at  $z$  closer to the reaction zone; including this extra point reduces the correlation coefficient and, thus, it should not have been included. Using the more reliable value of  $h_g = 4.35 \mu\text{m}$ , we follow the same procedure in calculating  $\Pi_{2D}$  for the experiments and use these values when comparing with the simulation results for  $\Pi_{2D}$  from Eq. (1). We emphasize that the simulation results for  $\Pi_{2D}(\phi_A)$  in Eq. (1) are independent of any value used for  $h_g$  in determining an experimental  $\Pi_{2D}(\phi_A)$ .

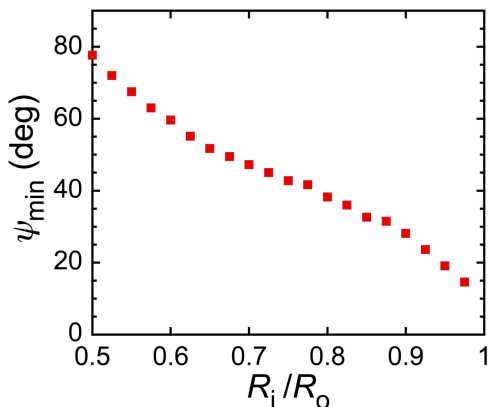


FIG. 4. Calculated minimum value of the opening angle  $\psi_{\min}$  of ASP shapes that can dimerize, as a function of  $R_i/R_o$ . In the region below this curve, dimerization is impossible.

Geometry limits the range of values of  $R_i/R_o$  and  $\psi$  over which dimerization of two separate monomer ASPs is physically possible, while keeping both ASPs in the plane while translating and rotating them. Dimerization can readily occur when the opening angle is large and the aspect ratio is sufficiently slender. Thus, at large  $\psi$  and  $R_i/R_o$ , dimerization is possible, but as  $\psi$  is reduced, or as the annular sector becomes thicker, corresponding to smaller  $R_i/R_o$ , dimerization is prohibited. These restrictions are quantified in Fig. 4, which displays the minimum value of  $\psi$  for which dimerization is possible, given a particular value of  $R_i/R_o$ . This value  $\psi_{\min}$  has been computed by numerically sampling the space of possible relative positions of two annular sectors, for given values of  $\psi$  and  $R_i/R_o$ . Here, we consider dimerization to be

physically possible if, in this space of relative positions, there exists an unbroken path between a un-dimerized configuration and a dimer state. This criterion excludes cases where the sectors would have to intersect one another in order to reach the dimer configuration, since these states are not physically realizable without lifting one of the sectors temporarily out of the plane. Although the simpler test for dimerization displayed in Fig. 1(b) is used for the actual enumeration of microstates in the cage model, the calculation of  $\psi_{\min}$  offers a definitive geometrical bound on the range of shape parameters for which the cage model remains meaningful.

Computed values of  $P_{\text{dimer}}$  using the two-particle simulation over a range of  $R_i/R_o$  and  $\psi$  are displayed in Figure 5. This probability is sensitive to changes in the slenderness of the ASPs, determined by  $R_i/R_o$ , as shown in Fig. 5(a). As  $R_i/R_o$  is increased towards unity, corresponding to increasing the slenderness of the ASP, dimerization can occur more readily at lower  $\phi_A$ . The thickness of the ends of the arms of ASPs relative to the opening angle is thus a key parameter related to insertion and dimerization; this controls the changes in  $\phi_A$  associated with the rise in  $P_{\text{dimer}}$  in Fig. 5(a). By contrast, in Fig. 5(b), we show that  $P_{\text{dimer}}(\phi_A)$  for fixed  $R_i/R_o = 0.75$  is not as sensitive to values of  $\psi$  over a limited range that corresponds to “C”-shapes. In this case, the differences between the curves is not as large, but the transition from low values of  $P_{\text{dimer}}$  to high values is much sharper for  $\psi = 70^\circ$  than for  $\psi = 110^\circ$ .

For  $R_i/R_o = 0.75$  and  $\psi = 95^\circ$ , near values that correspond to experiments [9], computed values of  $P_{\text{dimer}}$ ,  $K$ , and  $\Pi_{2D}$  from two-particle simulations are plotted as functions of  $\phi_A$  in Figs. 6(a), 6(b), and 6(c), respectively. We also show experimentally measured values of these quantities [9]. Fig. 6(a) also includes the values of  $P_{\text{dimer}}$  determined by the one-particle simulation, where one of the two central ASPs is fixed in position and orientation. We find good agreement between the experimental data and the two-particle simulation results for  $P_{\text{dimer}}$  and  $K$  for  $R_i/R_o = 0.75$  and  $\psi = 95^\circ$ . Small differences between experiment and simulation are noticeable at  $\phi_A$  greater than 0.28 for  $P_{\text{dimer}}$ , and at  $\phi_A$  greater than 0.34 for  $K$ . These differences at high  $\phi_A$  arise primarily because a small but non-negligible population of monomers becomes trapped in the experimental system, whereas the simulation assumes complete dimerization in the local cage. In the experimental system, diffusion of isolated trapped monomers in the crowded environment of dimers is extremely slow, and this kinetically inhibits further dimerization reactions of monomers that could lead to perfect dimerization. Moreover, the one-particle simulation performs poorly, compared to the two-particle simulation, in predicting the probability of dimerization, as shown by the larger departure from the experimental data in Fig. 6(a). Similar disagreement of the one-particle simulations in comparison with two-particle simulations and experiments are also observed for  $K$  and  $\Pi_{2D}$ . By contrast, the two-particle simula-

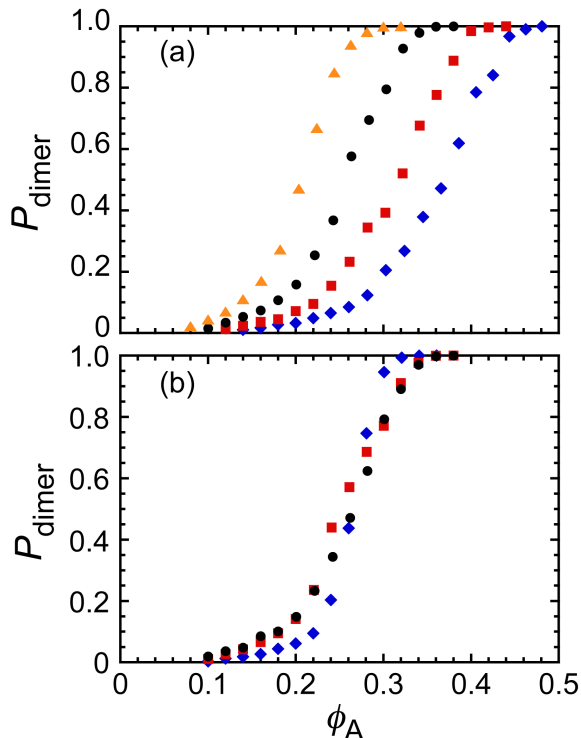


FIG. 5. Predictions from the two-particle cage model simulation of the dimerization probability  $P_{\text{dimer}}$ . **(a)**  $P_{\text{dimer}}$  as a function of  $\phi_A$  at fixed  $\psi = 100^\circ$ :  $R_i/R_o = 0.65$  (blue diamonds),  $R_i/R_o = 0.7$  (red squares),  $R_i/R_o = 0.75$  (black circles), and  $R_i/R_o = 0.8$  (orange triangles). **(b)**  $P_{\text{dimer}}$  as a function of  $\phi_A$  at fixed  $R_i/R_o = 0.75$ :  $\psi = 70^\circ$  (blue diamonds),  $\psi = 90^\circ$  (red squares), and  $\psi = 110^\circ$  (black circles).

tions of  $K$  and  $\Pi_{2D}$  nearly match the experimental results without any adjustable parameters over a large range of  $\phi_A$ , as shown in Figs. 6(b) and 6(c), respectively. At the highest  $\phi_A = 0.36$  shown, the two-particle simulation of  $K$  is much higher than the experimental  $K$ ; this is a predominantly a consequence of trapped monomers in the experiments, which causes a reduction in the experimental  $K$ . In Fig. 6(c), we have not reported simulated values of  $\Pi_{2D}$  at  $\phi_A = 0.34$  and  $\phi_A = 0.36$  because the discretization chosen for the simulations was not sufficiently fine to provide a large ensemble of accessible microstates. In addition, corner rounding, a consequence of diffraction in the experimental lithographic production of the particles, can cause the area fraction associated with the divergence in  $\Pi_{2D}$  to be different in the experiments than in the simulations, where no corner rounding is present. Thus, overall, the two-particle simulations agree reasonably well with experimental results, except at very high  $\phi_A$ , where trapped monomers are present in the experiments. This indicates that it is necessary to consider two mobile central ASPs, not a single central mobile ASP, in a static cage in order to obtain a reasonable representation of the entropy of the system. Consequently, we focus only on two-particle simulation

results for the remainder of this section.

The two-dimensional osmotic pressure varies linearly as a function of  $\phi_A$  for low particle area fractions, in the limiting case of an ideal gas, and it diverges at a maximum packing area fraction. This suggests the following functional form for the curve fit, where adjustable parameter  $f$  sets the overall scale, and the parameter  $\phi_{A,c}$ , a critical area fraction, sets the divergence point:

$$\Pi_{2D}(\phi_A)/(k_B T/A_p) = \frac{f\phi_A}{1 - \phi_A/\phi_{A,c}} \quad (3)$$

We fit the numerical results for the 2D scaled osmotic equation of state using this equation, as shown in Fig. 6(c), yielding very good agreement. Moreover, the fit parameter value of the divergence in the osmotic pressure,  $\phi_{A,c} = 0.47 \pm 0.01$ , is close to the experimental value  $\phi_{A,c} = 0.455$  previously reported [9]. Because we have used a thermal-gravitational height  $h_g = 4.35 \mu\text{m}$  here that is based on a more appropriate fit to the first few points of the initial rise of the measured monomer area fraction  $\phi_{A,M}(z)$  [9], the coefficient associated with the linear rise of the osmotic equation of state from the fit here is  $f = 2.5 \pm 0.1$ . This value is the same for both scaled numerical and scaled experimental results. However, corresponding to the different  $h_g$  used here, this coefficient is about thirty percent higher than  $f = 1.79$  reported in the prior experimental work. Regardless of experimental difficulty in precisely determining  $h_g$ , the shapes of the numerical and experimental scaled osmotic equations of state agree well over a wide range of particle area fractions.

To show the dependence of  $K$  on the scaled  $\Pi_{2D}$  from the two-particle simulations, we determine their values for each  $\phi_A$  in Figs. 6(b) and 6(c), and plot the results in Fig. 7. For  $10^{-1} \lesssim K \lesssim 10^2$ , we find that  $K$  exponentially increases with scaled  $\Pi_{2D}$ , so we fit this to:

$$K = \exp[(\Pi_{2D} - \Pi_{2D,\text{eq}})/\Pi_{2D}^*] \quad (4)$$

yielding fit parameter values of scaled  $\Pi_{2D,\text{eq}} = 1.5 \pm 0.1$  and  $\Pi_{2D}^* = 0.36 \pm 0.06$ . For larger values of scaled  $\Pi_{2D}$  beyond the range shown that are closer to the divergence in the scaled  $\Pi_{2D}(\phi_A)$ , we find that the simulated  $K$  departs from this simple exponential dependence and grows even more rapidly as the number of accessible monomer microstates approaches zero. This simulated exponential dependence matches experimental measurements well over the range shown [9]. While our simulations reveal  $\ln K \sim \Pi_{2D}$  for the ASP-pair dimerization reaction over a substantial range of scaled  $\Pi_{2D}$ , confirming prior experimental observations, this result could also be equivalently written as an exponential factor in a Poynting pressure correction to the fugacity of non-ideal hard ASP particles in a dense system [28]. The capacity of the hard ASPs to form interpenetrating lock-and-key dimer structures that are still compressible below close-packing densities is an interesting feature of this system.

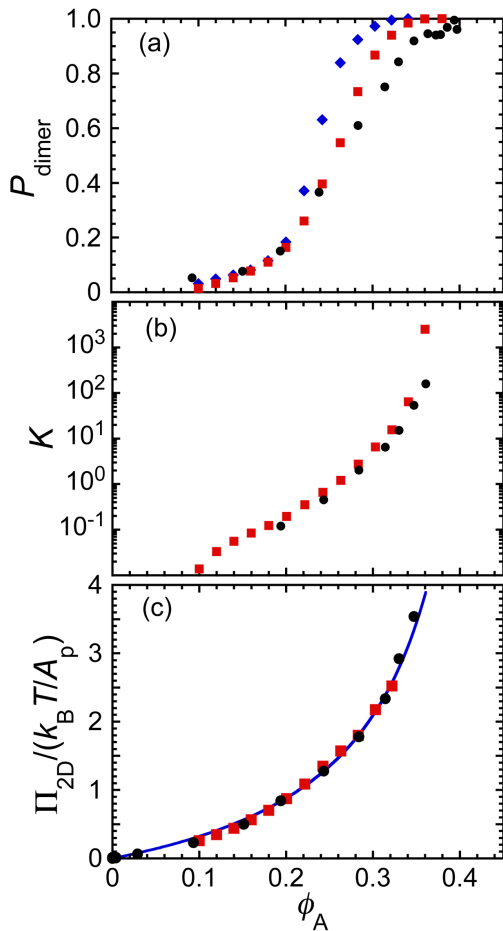


FIG. 6. Results of cage model simulations and experimental data as functions of  $\phi_A$ . (a) Probability of dimerization  $P_{\text{dimer}}$ : experiments (black circles), two-particle simulations (red squares), one-particle simulations (blue diamonds). (b) Equilibrium constant  $K$  of the dimerization reaction (same symbols). (c) Scaled 2D osmotic pressure  $\Pi_{2D}$  (same symbols). Line: fit to numerical results using Eq. (3) (see text).

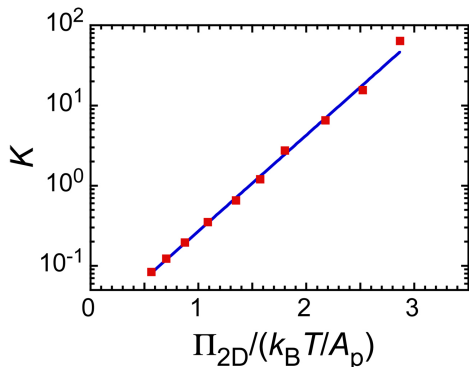


FIG. 7. Two-particle simulation results showing the dependence of the equilibrium constant,  $K$ , of the dimerization reaction as a function of the scaled 2D osmotic pressure,  $\Pi_{2D}$ . Solid line: fit using Eq. (4).

#### IV. CONCLUSION

Predictions based on the two-particle simulations agree well with experimental measurements made on a 2D Brownian system of ASPs, so a translational-rotational cage model containing two central mobile ASPs adequately captures the primary physical properties over a substantial range of  $\phi_A$ . By contrast, a cage model containing only a single mobile ASP surrounded by a fixed cage does not accurately predict the experimental results. This is an important finding, considering that single-particle translational-rotational cage models have proven to be useful for predicting structures that match experimental measurements reasonably well for other shapes, such as squares, tri-stars, and rhombs [14, 19, 21]. Therefore, when treating Brownian systems of shapes that can interpenetrate to a significant degree, such as hard ASPs, in order to obtain reasonable results using a cage model, a collective form of entropy that goes beyond a single-particle entropy serves as a reasonable starting point. Even so, the two-particle simulation still contains assumptions that do not exactly reflect the disordered racemic systems of ASPs that have been observed in the experiments. For instance, we have assumed that a perfectly regular dimer lattice is an appropriate cage and that equal maximal spacing between the perimeters of all of the ASPs in the cage reasonably approximates an average local state. This approximation can lead to differences between the predictions and experiments, especially at larger values of  $\phi_A$ . Moreover, because all cage ASPs are fixed and do not fluctuate in the two-particle simulations, we have considered only the six-dimensional phase space of two central mobile ASPs. This assumption of static cage ASPs represents an approximation that neglects other collective contributions to the system's entropy. Our results based on an assumed local structure of a cage could potentially be improved by considering an ensemble of cage structures that more closely mimic the randomness and variety in the chirality and orientation of cage ASPs seen in experiments. Ensemble-averaging over many different random cage configurations at the same density could improve predictions of the model towards lower  $\phi_A$ . Even the relationships between the microstate volumes  $\Omega$  and  $\Omega_D$ , and physical quantities such as  $P_{\text{dimer}}$ ,  $K$ , and  $\Pi_{2D}$ , are only strictly valid at thermodynamic equilibrium, and the experimental system contains defects and disorder that indicate the possibility of a state of the system that is not entirely its global minimum energy ground state. The success of the two-particle cage model of ASPs at reproducing the experimental data without any adjustable parameters suggests that this simplified model accurately captures many key features of the real system, despite these identifiable differences.

Given the success of the two-particle cage model in describing the physical behavior of a real 2D Brownian system of ASPs, simulation results using this two-particle cage model for other values of  $R_i/R_o$  and  $\psi$  serve as a pre-

dictive guide for future experiments on ASPs with a wider range of shape parameters. The predictions that we have presented here, which span a limited range of  $R_i/R_o$  and  $\psi$ , have been chosen to correspond to ranges in which the dominant behavior of dimerization is assumed to be present. The cage model that we have presented does not account for other non-dimer polymorphs of ASPs, such as polymeric chains, that have also been observed microscopically [9]. More complex modeling approaches would be required to account for a wider polymorphic diversity in reaction products, beyond simple dimers.

Many exciting future directions based on this work can be anticipated. For instance, microstates corresponding to single-penetration (Fig. 1(c)) could also be determined as a function of  $R_i/R_o$  and  $\psi$ , and the population of single-penetration configurations could be compared to those of non-penetrating and mutually interpenetrating configurations as a function of  $\phi_A$ . In addition, if one considers ASPs having  $\psi \approx \psi_{\min}$ , one could explore systems for which  $\psi$  becomes just large enough to allow dimerization; the behavior of this system should approach that

of disks when  $\psi$  drops well below  $\psi_{\min}$ . Likewise, reactions yielding different kinds of local polymorphs, such as chains in addition to dimers, over a broader range of  $R_i/R_o$  and  $\psi$  could be predicted through simulation and also explored experimentally. Numerically studying the impact of the effective size and shape of the central cavity resulting from a variety of disordered cages, each of which is consistent with the same  $\phi_A$ , could also reveal how sensitive or insensitive the two-particle predictions are to the exact geometries of the cages. Comparisons between the two-particle cage model results and other forms of simulation, such as molecular dynamics or Brownian dynamics, could also be made to determine higher-order corrections to the collective entropy.

## V. ACKNOWLEDGMENTS

The authors thank UCLA and the National Science Foundation (REU PHY-1460055) for financial support.

- 
- [1] Y. Fujii, H. Yamada, and M. Mizuta, *J. Phys. Chem.* **92**, 6768 (1988).
  - [2] C. Branden and J. Tooze, *Introduction to Protein Structure*, 2nd ed. (Garland Science, New York, 1999).
  - [3] J. B. Bancroft, G. J. Hills, and R. Markham, *Virology* **31**, 354 (1967).
  - [4] J. A. Speir, S. Munshi, G. Wang, T. S. Baker, and J. E. Johnson, *Structure* **3**, 63 (1995).
  - [5] J. K. Grimsley, J. M. Scholtz, C. N. Pace, and J. R. Wild, *Biochemistry* **36**, 14366 (1997).
  - [6] L. Onsager, *Ann. NY Acad. Sci.* **51**, 627 (1949).
  - [7] I. Langmuir, *J. Chem. Phys.* **6**, 873 (1938).
  - [8] C. J. Hernandez and T. G. Mason, *J. Phys. Chem. C* **111**, 4477 (2007).
  - [9] P. Y. Wang and T. G. Mason, *J. Am. Chem. Soc.* **137**, 15308 (2015).
  - [10] M. D. Hoover, S. A. Casalnuovo, P. J. Lipowicz, H. C. Yeh, R. W. Hanson, and A. J. Hurd, *J. Aerosol Sci.* **21**, 569 (1990).
  - [11] A. B. D. Brown, C. G. Smith, and A. R. Rennie, *Phys. Rev. E* **62**, 951 (2000).
  - [12] M. Sullivan, K. Zhao, C. Harrison, R. H. Austin, M. Megens, A. Hollingsworth, W. B. Russel, Z. Cheng, T. G. Mason, and P. M. Chaikin, *J. Phys.: Condens. Matter* **15**, S11 (2003).
  - [13] K. Zhao and T. G. Mason, *Phys. Rev. Lett.* **103**, 208302 (2009).
  - [14] K. Zhao, R. Bruinsma, and T. G. Mason, *Proc. Natl. Acad. Sci. U.S.A.* **108**, 2684 (2011).
  - [15] K. Zhao and T. G. Mason, *Phys. Rev. Lett.* **99**, 268301 (2007).
  - [16] T. G. Mason, *Phys. Rev. E* **66**, 060402 (2002).
  - [17] S. Asakura and F. Oosawa, *J. Chem. Phys.* **22**, 1255 (1954).
  - [18] S. Asakura and F. Oosawa, *J. Polym. Sci.* **33**, 183 (1958).
  - [19] K. Mayoral and T. G. Mason, *Soft Matter* **10**, 4471 (2014).
  - [20] K. Zhao and T. G. Mason, *J. Am. Chem. Soc.* **134**, 18125 (2012).
  - [21] K. Mayoral and T. G. Mason, *Entropic Self-Organization of Tri-Star Colloids* (Electrum Publishing, Los Angeles, 2013).
  - [22] W. B. Russel, D. A. Saville, and W. R. Schowalter, *Colloidal Dispersions* (Cambridge Univ. Press, Cambridge, 1989).
  - [23] L. Woodcock, *Ann. NY Acad. Sci.* **371**, 274 (1981).
  - [24] B. Widom, *Statistical Mechanics: A Concise Introduction for Chemists* (Cambridge Univ. Press, Cambridge, 2002).
  - [25] P. M. Chaikin and T. C. Lubensky, *Principles of Condensed Matter Physics* (Cambridge Univ. Press, Cambridge, 1995).
  - [26] D. C. Rapaport, *The Art of Molecular Dynamics Simulation*, 2nd ed. (Cambridge Univ. Press, Cambridge, 2004).
  - [27] I. N. Bronshtein, K. A. Semendyayev, G. Musiol, and H. Muhlig, *Handbook of Mathematics*, 5th ed. (Springer, Berlin, 2007).
  - [28] S. Sandler, *Chemical and Engineering Thermodynamics* (John Wiley and Sons, New York, 1977).